The plasticity shown here *in vitro* shares many properties with the plasticity observed *in vivo* following the pairing of a predictive signal with sensory input or intracellular current pulses[1–6]. In both cases, the changes are input-specific, bidirectional and established within a few minutes. In both cases the plasticity is anti-hebbian, with a decrease in excitation and a possible increase in inhibition taking place within a narrow temporal window. Thus, our results support the hypothesis that anti-hebbian plasticity at the parallel fibre synapse mediates the generation of negative images of predicted sensory input in these structures. □

Methods

400-μm thick slices of the mormyrid electrosensory lobe were maintained in an interface chamber in humidified 95% O_2, 5% CO_2 and superfused at room temperature (23–25 °C) with artificial cerebropsinal fluid (ACSF), at a rate of 2 ml min^{-1}. The ACSF was saturated with 95% O_2, 5% CO_2 and contained (in mM): NaCl 124; KCl 2.0; KH_2PO_4 1.25; $CaCl_2$ 2.6; $MgSO_4.7H_2O$ 1.6; $NaHCO_3$ 24; glucose 20. Two monopolar insulated tungsten stimulation electrodes were placed in the molecular layer (S1 and S2; inset in Fig. 1a) in order to stimulate two separate parallel fibre inputs to the recorded neurons (pulses of 0.1 ms and 5–50 μA amplitude). Purkinje-like cells were recorded intracellularly with sharp microelectrodes (150–200 MΩ) containing 2% biocytin dissolved in 2M potassium methyl sulphate. Paired pulse facilitation was measured in 7 cells at interpulse delays of 30–45 ms in order to test for activation of separate groups of fibres by S1 and S2. Facilitation was marked with stimulus pairs S1–S1 (range, 27–108%; mean, 54%) or S2–S2 (range, 18–69%; mean, 42%) but was minimal or absent with stimulus pairs S1–S2 (range, −7 to 13%; mean, −1.3%) or S2–S1 (range, −15 to 3%, mean, −3.6%), indicating that separate groups of fibres were stimulated.

Received 9 September 1996; accepted 24 March 1997.

1. Bell, C. An efference copy which is modified by reafferent input. *Science* **214,** 450–453 (1981).
2. Montgomery, J. & Bodznick, D. An adaptive filter than cancels self-induced noise in the electrosensory and lateral line mechanosensory systems of fish. *Neurosci. Lett.* **174,** 145–148 (1994).
3. Bastian, J. Pyramidal cell plasticity in weakly electric fish: A mechanism for attenuating responses to reafferent electrosensory inputs. *J. Comp. Physiol.* **176,** 63–78 (1995).
4. Montgomery, J., Coombs, S., Conley, R. & Bodznick, D. Hindbrain sensory processing in lateral line, electrosensory, and auditory systems: a comparative overview of anatomical and functional similarities. *Aud. Neurosci.* **1,** 207–231 (1995).
5. Bell, C., Caputi, A., Grant, K. & Serrier, J. Storage of a sensory pattern by anti-Hebbian synaptic plasticity in an electric fish. *Proc. Natl Acad. Sci. USA* **9,** 4560–4654 (1993).
6. Bell, C., Bodznick, D., Montgomery, J. & Bastian, J. The generation and subtraction of sensory expectations within cerebellum-like structures. *Brain, Behav. Evol.* (in the press).
7. Nelson, M. & Paulin, M. Neural simulations of adaptive reafference suppression in the elasmobranch electrosensory system. *J. Comp. Physiol. A* **177,** 723–736 (1995).
8. Meek, J. *et al.* Interneurons of the ganglionic layer of the mormyrid electrosensory lateral line lobe: morphology, immunocytochemistry and synaptology. *J. Comp. Neurol.* **375,** 43–65 (1996).
9. Grant, K. *et al.* Projection neurons of the mormyrid electrosensory lateral line lobe. *J. Comp. Neurol.* **375,** 18–42 (1996).
10. Sakurai, M. Synaptic modification of parallel fiber-Purkinje cell transmission in *in vitro* guinea-pig cerebellar slices. *J. Physiol.* **394,** 463–480 (1987).
11. Hirano, T. Differential pre- and postsynaptic mechanisms for synaptic potentiation and depression between a granule cell and a Purkinje cell in rat cerebellar cultures. *Synapse* **7,** 321–323 (1991).
12. Gustafsson, B., Wigström, H., Abraham, W. & Huang, Y. Long term potentiation in the hippocampus using depolarizing current pulses as the conditioning stimulus to single volley synaptic potentials. *J. Neurosci.* **7,** 774–780 (1987).
13. Debanne, D., Gähwiler, B. & Thompson, S. Asynchronous pre- and postsynaptic activity induces associative long-term depression in area CA1 of the rat hippocampus *in vitro*. *Proc. Natl Acad. Sci. USA* **91,** 1148–1152 (1994).
14. Stanton, P. & Sejnowski, T. Associative long term depression in the hippocampus induced by Hebbian covariance. *Nature* **339,** 215–218 (1989).
15. Hashemzadeh-Gargari, H., Colbert, C. & Levy, W. Refining the temporal defining of an association at the neuronal level using long-term potentiation and long-term depression in the dentate gyrus. *Neurosci. Lett.* **126,** 37–40 (1991).
16. Huerta, P. & Lisman, J. Bidirectional synaptic plasticity induced by a single burst during cholinergic theta oscillation in CA1 *in vitro*. *Neuron* **15,** 1053–1063 (1995).
17. Ito, M. Long term depression. *Annu. Rev. Neurosci.* 85–102 (1989).
18. Chen, C. & Thompson, R. Temporal specificity of long-term depression in parallel fiber-Purkinje synapses in rat cerebellar slice. *Learning Mem.* **2,** 185–198 (1995).
19. Ekerot, C. & Kano, M. Stimulation parameters influencing climbing fibre induced long-term depression of parallel fibre synpases. *Neurosci. Res.* **6,** 264–268 (1989).
20. Markram, H., Lübke, J., Frotscher, M. & Sakmann, B. Regulation of synaptic efficacy by coincidence of postsynaptic APs and EPSPs. *Science* **275,** 213–215 (1997).
21. Hebb, D. The organization of behavior. (Wiley, New York, 1949).

Acknowledgements. We thank Y. Fregnac for discussion and Y.F, N. Barmack and R. Kramis for critical reviews of the manuscript. This research was supported by grants from the NSF and the National Institute of Mental Health (to C.B.), by a contract from the European Economic Community, a grant from NATO and funds from the Centre National de Recherche Scientifique (to K.G.), and by grants from the del Duca Foundation and Yamada Science Foundation (to Y.S.).

Correspondence and requests for materials should be addressed to C.C.B. (e-mail: bellc@lhs.org).

Dynamics of orientation tuning in macaque primary visual cortex

Dario L. Ringach, Michael J. Hawken & Robert Shapley

Center for Neural Science, New York University, 4 Washington Place, New York, New York 10003, USA

Orientation tuning of neurons is one of the chief emergent characteristics of the primary visual cortex, V1 (refs 1, 2). Neurons of the lateral geniculate nucleus, which comprise the thalamic input to V1, are not orientation-tuned, but the majority of V1 neurons are quite selective. How orientation tuning arises within V1 is still controversial[1,3–17]. To study this problem, we measured how the orientation tuning of neurons evolves with time[18–20] using a new method: reverse correlation in the orientation domain. Orientation tuning develops after a delay of 30–45 milliseconds and persists for 40–85 ms. Neurons in layers 4Cα or 4Cβ, which receive direct input from the thalamus, show a single orientation preference which remains unchanged throughout the response period. In contrast, the preferred orientations of output layer neurons (in layers 2, 3, 4B, 5 or 6) usually change with time, and in many cases the orientation tuning may have more than one peak. This difference in dynamics is accompanied by a change in the sharpness of orientation tuning; cells in the input layers are more broadly tuned than cells in the output layers. Many of these observed properties of output layer neurons cannot be explained by simple feedforward models[1,3–6], whereas they arise naturally in feedback networks[7–17]. Our results indicate that V1 is more than a bank of static oriented filters; the dynamics of output layer cells appear to be shaped by intracortical feedback.

We adapted the reverse correlation method[21] to study the dynamics of orientation tuning in macaque V1. The stimulus was generated as follows. For each cell, a set S of sinusoidal gratings of a fixed spatial frequency but different orientations and spatial phases was generated. In these experiments, the orientation domain was sampled in steps ranging between 3° and 12°. For each orientation, sinusoidal gratings at four spatial phases a quarter of a cycle apart were included in the set. A stochastic image sequence (the stimulus) was generated by randomly selecting, at each video refresh time, a new image from S. This was done at a rate of 60 frames per second for a period of 15 min.

The data were analysed to determine the dependence of the cell's response on the past history of oriented gratings presented on its receptive field (Fig. 1). First, an array of counters corresponding to each of the orientations present in the stimulus was zeroed. A fixed value of a time-delay parameter τ was selected. For each nerve impulse recorded, we went back τ ms in time and obtained the orientation of the grating that was present at that moment in the image sequence. The counter corresponding to that orientation was incremented by one. Gratings at the same orientation but different spatial phases shared the same counter. Thus, this procedure averaged across spatial phases. When all action potentials were distributed in the counters, we normalized the resulting histogram by their total number and thereby obtained an estimate of the probability that an orientation θ was present in the stimulus image sequence τ ms before a nerve impulse was generated by the cell. This probability is denoted by $r_\tau(\theta)$. For a fixed value of τ, the function $r_\tau(\theta)$ is a probability distribution on the orientation angles present in the stimulus set. Note that this procedure is equivalent to that of computing the forward correlation: the probability of firing of a cell τ ms after the presentation of a particular orientation in the

stimulus sequence. We studied the dynamics of orientation tuning by looking at how the distributions $r_\tau(\theta)$ evolve with the time-delay parameter τ.

For $\tau = 0$, for example, we do not expect to see any influence of the input on the output train of action potentials because of the time delay between the retina and the evoked activity of cortical cells, so $r_\tau(\theta)$ should be a uniform distribution on the orientation domain. Similarly, for very long τ values we also expect to obtain a uniform distribution of $r_\tau(\theta)$; this is because cells have only finite memory. For intermediate values of τ, a smooth peaked distribution is expected which represents the preference of the cell for particular orientations. There will be one value of τ for which the cell will be better tuned than at any other time; we refer to this value as the 'optimal τ'.

We have applied this method to 61 cells of known laminar location in macaque V1. The results indicate two main patterns of dynamics: 'unimodal' and 'multimodal'. Unimodal dynamics mean that the orientation probability distribution develops from a uniform distribution into a smooth unimodal distribution until some optimal value of τ, and then relaxes back to uniform. Dynamical patterns that do not fit this description are referred to as being multimodal.

Figure 2a, b shows two cells with unimodal dynamics in layers 4Cα and 4Cβ. These distributions are broadly tuned for orientation; even at the optimal τ the probability that a cell responded to a grating at an orientation orthogonal to the preferred one is significantly larger than zero. All 12 cells studied in layers 4Cα and 4Cβ showed an evolution of the orientation probability distribution with unimodal dynamical characteristics like those shown in Fig. 2a, b.

Multimodal dynamics (Fig. 2c–h) were observed in 28 out of 49 cells in supragranular and infragranular layers. The laminar distribution of these cells is summarized in Table 1. Figure 2c illustrates multimodal dynamics in one sharply orientation-tuned neuron from layer 4B. The orientation distribution for this cell at $\tau = 53$ ms before a spike occurred is narrow with a single peak; this peak corresponds to the best orientation as measured with steady state drifting sine gratings. For a time delay of $\tau = 59$ ms, the shape of the probability function is not single-peaked but rather resembles a Mexican hat in the orientation domain: the orientations flanking the optimum orientation became relatively less effective in eliciting a response[22]. The distribution changes at 71 ms, where the orientation probability function shows a broad peak at an orientation orthogonal to that measured at $\tau = 53$ ms. This means that with a 71-ms delay, the most likely orientation to precede a nerve impulse is orthogonal to the main peak measured at shorter delays. Such dynamical shifts between the preferred and the orthogonal orientation, when going from short to long delay times, were a common finding outside layer 4C. All cells classified as multimodal showed such an 'inversion' of the orientation distribution to some extent. Another example of such an inversion in the orientation distributions of a layer 4B cell is shown in Fig. 2d.

We also observed other patterns of multimodal dynamics, for example, cells whose preferred orientation seemed to drift continuously with time[19]. These cells were mainly found in layers 2 + 3 and 5. Figure 2e shows the result obtained from a cell in layer 2 + 3. At a time delay of $\tau = 56$ ms, the best orientation is about 130°, and in the subsequent graphs the peak shifts towards 180° (64 ms), winds around zero degrees (72 ms), and then remains stable at 60° for $\tau \geq 88$ ms. Notice that at $\tau = 88$ ms, the distribution has a mode 90° away from the mode of the distribution at $\tau = 56$ ms. Therefore this cell also exhibits an inversion of the orientation distribution. Similar results from a cell in layer 5 are depicted in Fig. 2f: the preferred orientation of this cell at $\tau = 54$ ms is around 120°, at $\tau = 75$ ms it shifted to 90°, and by $\tau = 82$ ms the peak moved to 55°. Figure 2g shows a very sharply tuned cell in layer 2 + 3. The probability distribution profiles of this cell have a Mexican hat shape for almost the entire period of the cell's response. The orientations flanking the optimal one have the lowest probability of preceding a spike. At 122 ms, the neuron exhibits an inversion of the distribution. Finally, a particular type of dynamics is observed in some neurons of layer 6 (Fig. 2h): a single-peaked distribution develops until $\tau = 59$ ms, but for time delays larger than 59 ms the distributions become clearly double-peaked. The modes are ~90° away, corresponding to orthogonal orientations[22,23]. The secondary peak even becomes dominant at $\tau = 91$ ms.

The change in the dynamics of orientation tuning, from unimodal to multimodal observed when moving from layer 4C to supragranular and infragranular layers is accompanied by a sharpening of orientation tuning. Cells in layer 4C, which all have unimodal dynamics, are more broadly tuned than cells in other layers[24,25]. This can already be seen in the examples shown in Fig. 2. We also measured the orientation tuning bandwidth in a relatively large population of $N = 316$ cells (39 located in 4Cα, 37 in 4Cβ, and 240 outside layer 4C) using conventional drifting sinewave gratings. Orientation bandwidth was characterized by the circular variance of the responses[25] (see Methods). We found that cells in 4C are significantly less tuned than cells outside layer 4C (Wilcoxon

Table 1 Laminar distribution of cells with 'multimodal' dynamics

Layer	Total cells	'Multimodal'	Percentage
2 + 3	18	7	39
4B	12	11	91
4C	12	0	0
5	9	5	56
6	10	5	50

The total number of cells sampled in each layer and the number and percentage of these cells that exhibited 'multimodal' dynamics are shown. All cells in layer 4C had unimodal dynamics. The largest concentration of multimodal cells is in layer 4B. We have not yet sampled from cells in layer 4A.

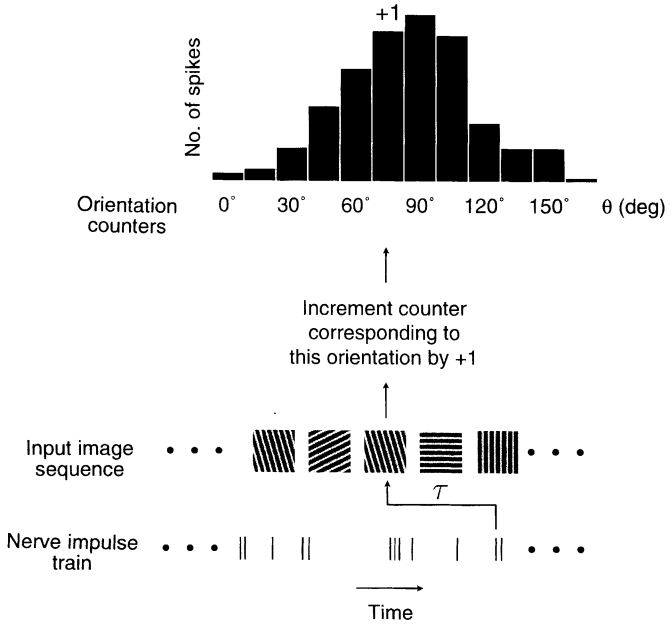

Figure 1 Reverse correlation in the orientation domain. A fast sequence of gratings with a fixed spatial frequency but random orientations and spatial phases is presented in the cell's receptive field. A segment showing five consecutive frames in such a sequence is shown in the figure. The number of times a particular orientation was present in the stimulus sequence τ ms before a spike occurred is shown by the histogram. Normalizing the histogram by the total number of spikes, we obtain an estimate of $r_\tau(\theta)$, the probability that a grating with orientation θ was present in the stimulus τ ms before an action potential was recorded. We study the dynamics of orientation tuning by looking at the evolution of $r_\tau(\theta)$ with τ.

rank sum test, $Z = 4.91$, $P < 5 \times 10^{-7}$; the median circular variance in layer 4C was 0.77, and for cells outside 4C was 0.41).

Simulations we have performed of simple feedforward networks based on spatially aligned lateral geniculate nucleus-like inputs (with identical time-course responses for all subunits) show unimodal dynamics (M. Pugh, M. Shelley, D. McLaughlin, R.S. and D.L.R., unpublished observations). The orientation distributions observed outside layer 4C are difficult to reconcile with such a feedforward model. In contrast, some features of the multimodal dynamics arise naturally in recurrent feedback networks[15–17] (M. Carandini and D.L.R., manuscript in preparation). For instance, inversions of the orientation distributions may occur if neurons with orthogonal orientation preferences inhibit each other[26]. Centre-surround facilitation and suppression in the orientation domain[15–17] may account for the secondary peaks seen in distributions like those of the layer 6 cell in Fig. 2h, and the Mexican hat shape of the orientation probability functions in Fig. 2c, g.

The dynamics observed outside layer 4C can be described as having two components: an oriented early excitatory component followed by a delayed inhibitory or suppressive component with similar preferred orientation but broader orientation tuning. This suppression will sharpen the steady-state orientation tuning of a cell. In some cases (Fig. 2g), the inhibitory component appears quite rapidly and may have an immediate effect on the orientation tuning properties of the cell. It is possible that a more complicated feedforward mechanism than the one we considered is responsible for generating the delayed inhibitory component. However, a simple mechanism like a hyperpolarization of the cell following a recent excitation does not account for most of the dynamical features in the data, such as the Mexican hat distributions or the drifts in the preferred orientation of the cell with time. Long-range lateral interactions between centre and surround could also be contributing to the dynamics or orientation tuning observed in our experiments[27–29].

We have observed five cells whose orientation tuning bandwidth decreased with time during the early phase of the response[20]. In Fig. 3a, normalized distributions from a neuron in layer 2 + 3 for two delay times, $\tau = 45$ ms and 55 ms are shown. There is a clear progression from broad to sharper orientation tuning with time. Figure 3b, c shows further examples from layer 2 + 3 and layer 5. In all cases, sharpening occurred quite rapidly, within 6 − 10 ms. This phenomenon might be caused in a recurrent network if the

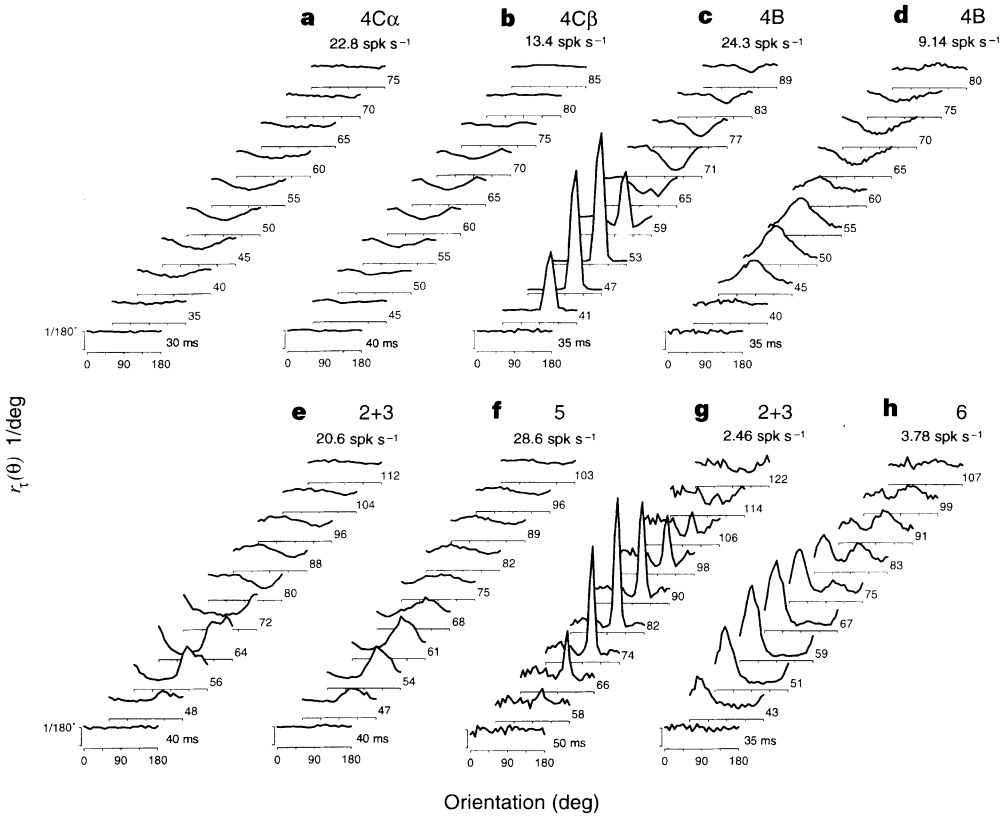

Figure 2 The dynamics of orientation tuning in V1. The graphs within each column show the evolution of the probability distribution function $r_\tau(\theta)$ with τ. The value of τ is written beside each graph. In all panels the x-axis represents orientation between 0° and 180°. The y-axis represents the value of the probability density function $r_\tau(\theta)$ for the values of τ indicated. Notice that a uniform distribution has a constant value of 1/180° as indicated by the vertical scale at the bottom graph in each column. All graphs have the same vertical scale. As $r_\tau(\theta)$ is a distribution on the orientation angles for any τ, the integral under all the curves is constant and equal to one. In each case, the distributions $r_\tau(\theta)$ were uniform up until the first τ shown. The laminar location of each cell and its mean firing rate during the stimulation period are indicated at the top. **a**, **b**, Cells in layer 4Cα and 4Cβ show unimodal dynamics and are more broadly tuned than cells in supragranular and infragranular layers. **c**, the result from a cell in layer 4B which is sharply tuned at $\tau = 53$ ms, has a Mexican hat distribution profile at 59 ms, and shows an inversion at 71 ms. **d**, A cell in layer 4B which shows a large inversion of the distribution. **e**, **f**, Cells in layers 2 + 3 and 5 whose preferred orientation drifted continuously with time. **g**, A sharply tuned cell in layer 2 + 3 whose orientation distribution profile resembles a Mexican hat for most of the response period of the neuron. **h**, Dynamics of a cell in layer 6 which shows the appearance of a secondary peak at the orthogonal orientation for $\tau \geq 67$ ms.

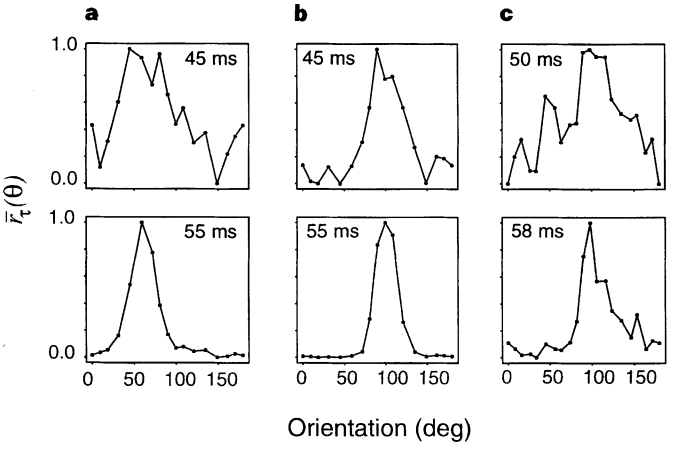

Figure 3 The sharpening of orientation tuning over time. For each given τ, the distribution $r_\tau(\theta)$ was normalized as follows; $\bar{r}_\tau(\theta) = \{r_\tau(\theta) - \min(r_\tau(\theta))\}/\{\max(r_\tau(\theta)) - \min(r_\tau(\theta))\}$; where the minimum and the maximum are taken over the orientation θ. Normalization is required to compare the tuning of the responses independently of their magnitude. Each column in this figure represents the normalized distributions of a cell at two values of τ. **a**, **b**, Examples of two cells in layer 2 + 3 for which the normalized distributions sharpen over time. **c**, The sharpening effect on a cell in layer 5. This kind of sharpening could be due to recurrent excitatory amplification of the responses at the preferred orientation of the cell[16].

sharpening effect of intracortical feedback is slightly delayed with respect to the input[20].

A new and surprising result is that the dynamics of orientation tuning in layer 4C of macaque V1 are quite different from the dynamics in the supragranular and infra-granular layers. The dynamics seen outside layer 4C may be essential in determining the orientation tuning properties of these cells, and could be involved in the encoding of subtler spatial features of the visual image. □

Methods

Acute experiments were performed on adult Old-World monkeys (*Macaca fascicularis*). Animals were initially tranquilized with i.m. acepromazine (50 μg kg^{-1}), anaesthetized with i.m. ketamine and maintained on i.v. opioid anaesthetic (sufentanil citrate, 6 μg kg^{-1} h^{-1}). During recording, anaesthesia was continued with sufentanil (6 μg kg^{-1} h^{-1}) and paralysis induced with pancuronium bromide. Electrocardiogram and expired CO_2 were continuously monitored and blood pressure was measured non-invasively at intervals of 5 min by a Hewlett-Packard Model 78354A patient monitor. Extracellular action potentials were recorded with glass-coated tungsten microelectrodes, exposed tips 5–15 μm. Spikes were detected using a Bak (Maryland, USA) DDIS-I dual window discriminator and were time-stamped with an accuracy of 1 ms using a CED-1401 Plus (Cambridge, UK) data acquisition system. Strict criteria for single-unit recording included fixed shape of the action potential and the absence of spikes during the absolute refractory period. Small electrolytic lesions (2–3 μA for 2–3 s, tip negative) were made along the length of each penetration. Details of the reconstruction of the penetrations and the assignment of cells to cortical layers can be found in ref. 30.

A Silicon Graphics Elan R4000 computer generated the stimuli in real time. The screen measured 34.3 cm wide by 27.4 cm high. The refresh rate of the monitor was 60 Hz. The mean luminance of the display was 56 cd m^{-2}. The contrast of the gratings was 100% and their spatial frequency was optimal for each cell. The size of the stimulation patch was large compared to the receptive field of the cell; the side of the stimulus was between 6 and 10 times the spatial period of the optimal grating. The receptive field of the cell was centred in the middle of the stimulus. Therefore, both the classical receptive field of the cell and its surround were stimulated. Most cells responded with mean spike rates ranging between 2 and 40 spikes per second. A few cells with very high directional selectivity did not respond at all to the stimulus and could not be studied.

We ran stimulus sequences for 15 min (900 s or 54,000 frames). In a typical experiment we used an angular resolution of ~10°. Thus, the set S usually contained 72 different images (18 orientations × 4 spatial phases). During the 15-min presentation each image appeared, on average, 750 times. If a typical cortical neuron fired ~5 spikes per second to the stochastic stimulation sequence, we obtained a total of 4,500 spikes. We distributed these 4,500 spikes in only 18 orientation bins (because we average across spatial phases). Thus, for a uniform distribution, about 250 spikes are found in each bin. The large number of spikes and small number of orientation bins allowed us to obtain smooth and accurate orientation probability distributions.

The circular variance V of a cell which has responses R_k at angles $0° \le \theta_k < 180°$ is given by $V = 1 - \frac{|\Sigma_k R_k \exp(i2\theta_k)|}{\Sigma_k R_k}$. Circular variance is a measure of orientation bandwidth which is bounded between zero and one. Cells not tuned for orientation have a circular variance of one. Cells that are very sharply tuned have circular variance values close to zero.

Received 4 December 1996; accepted 7 March 1997.

1. Hubel, D. H. & Wiesel, T. N. Receptive fields, binocular interaction and functional architecture of cat's visual cortex. *J. Physiol. (Lond.)* **160,** 106–154 (1962).
2. Hubel, D. H. & Wiesel, T. N. Receptive fields and functional architecture of monkey striate cortex. *J. Physiol. (Lond.)* **195,** 215–245 (1968).
3. Chapman, B. *et al.* Relation of cortical cell orientation selectivity to alignment of receptive fields of the geniculocortical afferents that arborize within a single orientation column in ferret visual cortex. *J. Neurosci.* **11,** 1347–1358 (1991).
4. Ferster, D. Orientation selectivity of synaptic potentials in neurons of cat primary visual cortex. *J. Neurosci.* **6,** 1284–1301 (1986).
5. Ferster, D. *et al.* Orientation selectivity of thalamic input to simple cells of cat visual cortex. *Nature* **380,** 249–252 (1996).
6. Reid, R. C. & Alonso, J. M. Specificity of monosynaptic connections from thalamus to visual cortex. *Nature* **378,** 281–284 (1995).
7. Andrews, D. P. Perception of contours in the central fovea. *Nature* **205,** 1218–1220 (1965).
8. Blakemore, C. *et al.* Lateral inhibition between orientation detectors in the human visual system. *Nature* **228,** 37–39 (1970).
9. Benevento, L. A. *et al.* Significance of intracortical inhibition in the visual cortex. *Nature* **238,** 124–126 (1972).
10. Henry, G. H. *et al.* Orientation specificity of cells in cat striate cortex. *J. Neurophysiol.* **37,** 1394–1409 (1974).
11. Sillito, A. M. *et al.* A re-evaluation of the mechanisms underlying simple cell orientation selectivity. *Brain Res.* **194,** 517–520 (1980).
12. Bonds, A. B. Role of inhibition in the specification of orientation selectivity of cells in the cat striate cortex. *Visual Neurosci.* **2,** 41–55 (1989).
13. Nelson, S. B. Temporal interactions in the cat visual system. I. Orientation-selective suppression in the visual cortex. *J. Neurosci.* **11,** 344–356 (1991).
14. Wörgötter, F. & Koch, C. A detailed model of the primary visual pathway in the cat: comparison of afferent excitatory and intracortical inhibitory connection schemes for orientation selectivity. *J. Neurosci.* **11,** 1959–1979 (1991).
15. Somers, D. C., Nelson, S. B. & Sur, M. An emergent model of orientation selectivity in cat visual cortical simple cells. *J. Neurosci.* **15,** 5448–5465 (1995).
16. Douglas, R. J. *et al.* Recurrent excitation in neocortical circuits. *Science* **269,** 981–985 (1995).
17. Ben-Yishai, R. *et al.* Theory of orientation tuning in the visual cortex. *Proc. Natl Acad. Sci. USA* **92,** 3844–3848 (1995).
18. Celebrini, S. *et al.* Dynamics of orientation coding in area V1 of the awake primate. *Visual Neurosci.* **10,** 811–825 (1993).
19. Shevelev, I. A. *et al.* Dynamics of orientation tuning in the cat striate cortex neurons. *Neuroscience* **56,** 865–876 (1993).
20. Pei, X. *et al.* Receptive field analysis and orientation selectivity of postsynaptic potentials of simple cells in cat visual cortex. *J. Neurosci.* **14,** 7130–7140 (1994).
21. de Boer, E. & Kuyper, P. Triggered correlation. *IEEE Trans. Biomed. Enging.* **15,** 169–179 (1968).
22. DeValois, R. L. *et al.* The orientation and direction selectivity of cells in macaque visual cortex. *Vision Res.* **22,** 531–544 (1982).
23. Shevelev, I. A. *et al.* Double orientation tuning in the cat visual cortex units. *Neuroscience* **61,** 965–973 (1994).
24. Blasdel, G. G. & Fitzpatrick, D. Physiological organization of layer 4 in macaque striate cortex. *J. Neurosci.* **4,** 880–895 (1984).
25. Leventhal, A. G. *et al.* Concomitant sensitivity to orientation, direction, and color of cells in layers 2, 3, and 4 of monkey striate cortex. *J. Neurosci.* **15,** 1808–1818 (1995).
26. Morrone, M. C. *et al.* Functional implications of cross-orientation inhibition of cortical visual cells. I. Neurophysiological evidence. *Proc. R. Soc. Lond. B* **216,** 335–354 (1982).
27. Lund, J. S. Anatomical organization of macaque monkey striate visual cortex. *Annu. Rev. Neurosci.* **11,** 253–288 (1988).
28. Blakemore, C. & Tobin, E. A. Lateral inhibition between orientation detectors in the cat's visual cortex. *Exp. Brain Res.* **15,** 439–440 (1972).
29. Sillito, A. M. *et al.* Visual cortical mechanisms detecting focal orientation discontinuities. *Nature* **378,** 492–496 (1995).
30. Hawken, M. J. *et al.* Laminar organization and contrast sensitivity of direction-selective cells in the striate cortex of the Old World monkey. *J. Neurosci.* **8,** 3541–3548 (1988).

Acknowledgements. This work was supported by the NIH (R.S and M.J.H.) and the Sloan Foundation. We thank M. Carandini, K. Gegenfurtner, J. Krauskopf, M. Landy, F. Mechler, N. Rubin, G. Sapiro and E. Simoncelli for comments on the manuscript. Part of the data obtained using drifting sinewave gratings was collected by A. J. Parker and M. J. Hawken at Oxford University.

Correspondence and requests for materials should be addressed to D.L.R. (e-mail: dario@cns.nyu.edu).